Synthesis Method for Even-Order Symmetrical Chebyshev Bandpass Filters With Alternative J/K Inverters and $\lambda/4$ Resonators

Songbai Zhang, *Student Member, IEEE*, and Lei Zhu, *Fellow, IEEE*

***Abstract*—This paper proposes a unified synthesis method for the bandpass filters based on the alternative J/K inverters and $\lambda/4$ microstrip line resonators. Firstly, an even-order Chebyshev bandpass filter prototype with equal terminations is transformed to two dual networks based on hybrid J/K inverters and $\lambda/4$ resonators. In this work, two adjacent $\lambda/4$ resonators are coupled with each other through a semi-lumped via-hole as the K inverter; the tailored method is employed and effectively demonstrated to extract the J/K inverters' values and their respective associated effective lengths. As its application examples, the proposed synthesis method is applied to design two classes of even-order Chebyshev bandpass filters with fourth and sixth order on microstrip-line topology, which operate at 2.4 GHz with the fractional bandwidths of 10% and 15%, respectively. Finally, both classes of filters are fabricated and measured. Simulated and measured results provide a good verification for the theoretical counterparts.**

***Index Terms*—Bandpass filter, even-order symmetrical Chebyshev bandpass filter, quarter-wavelength resonators and synthesis method.**

I. Introduction

MICROWAVE bandpass filters based on $\lambda/4$ resonators possess several attractive features, such as compact size, relaxed inter-resonator coupling, and wide upper stopband. In [1], a prominent $\lambda/4$ resonator interdigital bandpass filter was developed where each resonator had its own ground. Fig. 1(a) and (b) portrays the schematics of two conventional Chebyshev bandpass filter prototypes with third and fourth order, respectively [2]. In these networks, three or four $\lambda/4$ resonators are cascaded in series by alternative J and K inverters. Since J and K inverters could both be easily implemented on the uniplanar coplanar waveguide (CPW) structure, there were plenty of examples of bandpass filters designed and fabricated on a CPW structure [3]–[6]. In particular, this kind of filter was widely used for exploration of high-temperature superconductor (HTS) filters [7], [8] and the millimeter-wave integrated filter [5]. On the other hand, two second-order microstrip bandpass filters were proposed based on $\lambda/4$ resonators in the alternative J–K–J form [9] and [10]. In [9], the K inverter was implemented with a shunt open-end stub with a length shorter or longer than the $\lambda/4$, whereas a via-hole was employed to function as a simple K inverter in [10]. Following the work in [10], a few compact fourth-order microstrip bandpass filters were reportedly constituted with quasi-elliptic functionality [11] and widened upper stopband [12]. Using the $\lambda/4$ stepped-impedance resonators (SIRs), compact filters with improved upper stopband performance were demonstrated in [13] and [14], and a dual-band bandpass filter was presented in [15] with the use of the first two resonant modes in the $\lambda/4$ SIRs in the J–K–J form. However, only even-order Butterworth frequency responses were achieved in [11], [12], and [15], although a few fourth-order filters on the specified quadruplet topology were designed on CPW [5] and microstrip line [16] topologies. Bandpass filters designed in [11]–[16] in fact heavily depends on the extensive tuning and optimization via the full-wave simulator rather than the expected synthesis method. No reported works really systematically addressed the synthesis design for the symmetrical bandpass filter based on the $\lambda/4$ resonators.

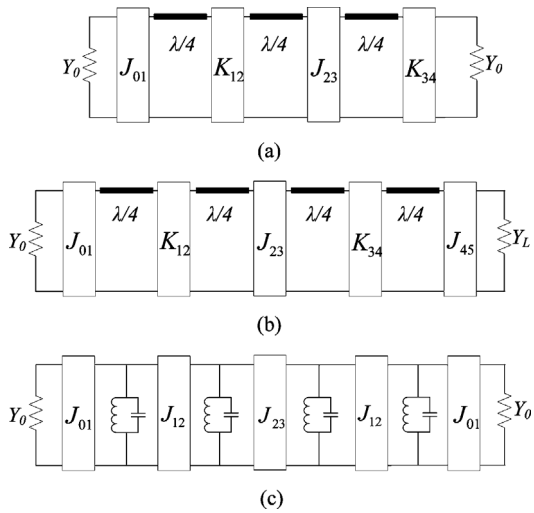

Fig. 1. (a) and (b) Conventional third- and fourth-order Chebyshev bandpass filter prototypes based on $\lambda/4$ resonators with equal and unequal source/load admittances, respectively. (c) Symmetrical fourth-order Chebyshev bandpass filter prototype with equal source/load admittances.

Firstly, an odd-order, e.g., third-order, Chebyshev bandpass filter with alternative J/K inverters is investigated, as shown in Fig. 1(a). This filter is formed by the sequence of J–K–J–K inverters so it is a nonsymmetrical two-port network since the input port and first resonator is coupled by a J inverter, while

Manuscript received November 12, 2012; accepted November 15, 2012. Date of publication December 21, 2012; date of current version February 01, 2013.

The authors are with the School of Electrical and Electronic Engineering, Nanyang Technological University, Singapore 639798 (e-mail: szhang3@e.ntu.edu.sg; ezhul@ntu.edu.sg).

Color versions of one or more of the figures in this paper are available online at http://ieeexplore.ieee.org.

Digital Object Identifier 10.1109/TMTT.2012.2233748

the output port and third resonator is coupled by a K inverter. Fig. 1(b) shows a conventional even-order bandpass filter with the order of $N = 4$. Due to the complete circle of J–K–J–K–J inverters, this filter network itself is symmetrical in its topology. However, to achieve the Chebyshev frequency response, the output admittance Y_L is unequal to the input admittance Y_0 since normalized g_{N+1} is not equal to unity. Thus, an additional impedance transformer needs to be installed at the output port if the synthesis method in [1] is applied to design this even-order filter with a Chebyshev frequency response. In this work, the symmetrical even-order Chebyshev filter prototype with equal I/O admittance is constructed based on [17], as the fourth-order one is exemplified as shown in Fig. 1(c).

This paper primarily aims to transform the symmetrical Chebyshev bandpass prototype with shunt LC resonant tanks and J inverters in Fig. 1(c) to the network based on alternative J/K inverters and $\lambda/4$ resonators. In practice, the $\lambda/4$ resonators are coupled via a co-shared semi-lumped K inverter that is realized by a via-hole in microstrip technology. By tuning the via-hole diameter, the prescribed inter-resonator coupling strength and external quality value (Q_e) can be achieved, while the resonant frequencies of two coupled $\lambda/4$ resonators are significantly changed. As a result, the conventional Dishal's method [18] for the filter's physical dimension derivation, as detailed in [19], is not applicable. Therefore, a unified synthesis method is proposed to explicitly extract the physical dimensions of each individual J and K inverters and the resonators' structures.

This paper is organized as follows. In Section II, two dual types of filter networks transformed from either all J inverters or all K inverters networks are firstly synthesized. Next, the detail filter dimension derivation method is formulated. Subsequently, the fourth-order microstrip bandpass filters centered at 2.4 GHz with the fractional bandwidth of 10% are synthesized and discussed in Section III. Section IV presents the example of sixth-order microstrip-line bandpass filter at 2.4 GHz with a fractional bandwidth of 15%. Lastly, Section V concludes this paper.

II. Network Transformation and Filter Dimension Derivation

A. Network Transformation

The first step is to transform the bandpass filter prototypes in the forms of shunt LC resonators and J inverters in Fig. 2(a) or series LC resonators and K inverters in Fig. 3(a) to the prototypes based on the alternative J/K inverter and $\lambda/4$ resonators, respectively. As illustrated in Figs. 2 and 3, the $ABCD$ matrices at the exact resonant frequency among different topologies between two reference planes R_1 and R_2 should be equal to each other. From Fig. 2, (1) can be easily derived,

$$\begin{bmatrix} 0 & \frac{j}{J_{n,n+1}} \\ jJ_{n,n+1} & 0 \end{bmatrix} = \begin{bmatrix} 0 & -j\frac{Z_nZ_{n+1}}{K_{n,n+1}} \\ -jY_nY_{n+1}K_{n,n+1} & 0 \end{bmatrix} \tag{1}$$

where Z_n, Y_n, Z_{n+1}, and Y_{n+1} are the characteristic impedances and admittances of the two neighboring $\lambda/4$ resonators.

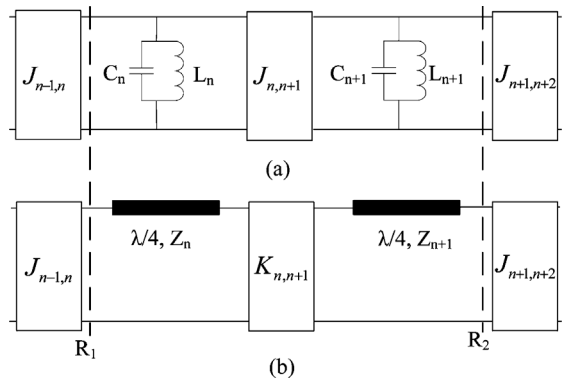

Fig. 2. (a) Bandpass filter network based on shunt-parallel LC resonators and J inverters. (b) Transformed bandpass filter network segment with $\lambda/4$ transmission lines and alternative J/K inverters.

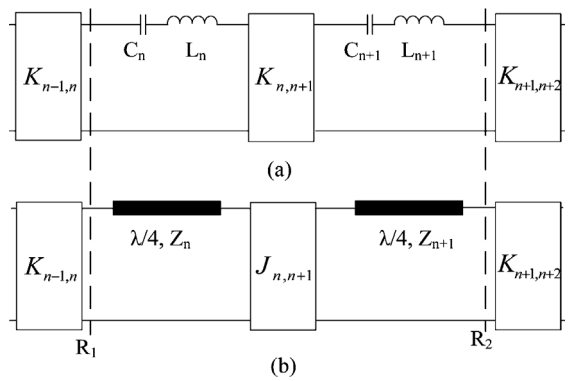

Fig. 3. (a) Bandpass filter network based on series LC resonators and K inverters. (b) Transformed bandpass filter network segment with $\lambda/4$ transmission lines and alternative J/K inverters.

Alternatively, (2) for its dual network shown in Fig. 3 at the exact resonant frequency is derived as follows:

$$\begin{bmatrix} 0 & jK_{n,n+1} \\ \frac{j}{K_{n,n+1}} & 0 \end{bmatrix} = \begin{bmatrix} 0 & -jZ_nZ_{n+1}J_{n,n+1} \\ -j\frac{Y_nY_{n+1}}{J_{n,n+1}} & 0 \end{bmatrix}. \tag{2}$$

Both (1) and (2) can be further simplified as (3),

$$-\frac{K_{n,n+1}}{\sqrt{Z_nZ_{n+1}}} = \frac{J_{n,n+1}}{\sqrt{Y_nY_{n+1}}}. \tag{3}$$

For a synchronous-tuned filter on uniform $\lambda/4$ resonators,

$$-\frac{K_{n,n+1}}{Z_r} = \frac{J_{n,n+1}}{Y_r} \tag{4}$$

where Z_r and Y_r are the characteristic impedance and admittance of the $\lambda/4$ resonators.

The $\lambda/4$ resonator behaves like either a shunt LC resonator looking from its open-circuited end or a series LC resonator looking from its short-circuited end. Hence, the susceptance slope b_r and reactance slope x_r can be calculated at its resonant frequency with reference to their equivalent lumped shunt or series LC resonant circuits as

$$b_r = \frac{\pi Y_r}{4} \tag{5}$$

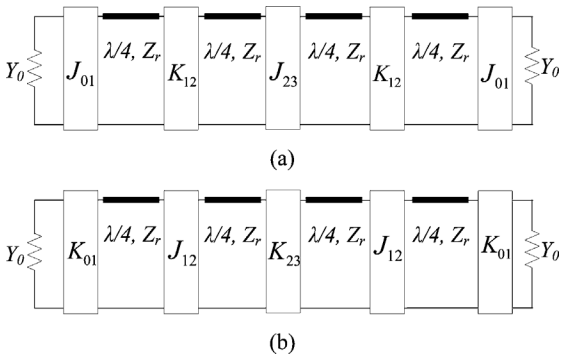

Fig. 4. Fourth-order symmetrical Chebyshev bandpass filter network with equal terminations on $\lambda/4$ resonators starting with: (a) J inverter and (b) K inverter.

and

$$x_r = \frac{\pi Z_r}{4}. \tag{6}$$

The fourth-order Chebyshev bandpass filter with equal source and load admittances in Fig. 1(c) can now be transformed to the desired network in Fig. 4(a). The values of corresponding J/K inverters are calculated with (4) and (5) by taking the low-pass cutoff frequency $\Omega_c = 1$,

$$\frac{J_{01}}{\sqrt{Y_0 Y_r}} = \sqrt{\frac{\mathrm{FBW}\pi}{4g_0 g_1}} \tag{7a}$$

$$-\frac{K_{12}}{Z_r} = \frac{J_{12}}{Y_r} = \frac{\mathrm{FBW}\pi}{4}\sqrt{\frac{1}{g_1 g_2}} \tag{7b}$$

$$\frac{J_{23}}{Y_r} = \frac{\mathrm{FBW}\pi}{4}\sqrt{\frac{1}{g_2 g_3}} \tag{7c}$$

where FBW is the fractional bandwidth and g_n are the first four elements of the fourth-order Chebyshev low-pass prototype. By performing the transformation on its dual network based on series *LC* resonators and K inverters shown in Fig. 3(a), the resultant network can be derived as shown in Fig. 4(b). The associated J/K values are then calculated based on (4) and (6),

$$\frac{K_{01}}{\sqrt{Z_0 Z_r}} = \sqrt{\frac{\mathrm{FBW}\pi}{4g_0 g_1}} \tag{8a}$$

$$-\frac{J_{12}}{Y_r} = \frac{K_{12}}{Z_r} = \frac{\mathrm{FBW}\pi}{4}\sqrt{\frac{1}{g_1 g_2}} \tag{8b}$$

$$\frac{K_{23}}{Z_r} = \frac{\mathrm{FBW}\pi}{4}\sqrt{\frac{1}{g_2 g_3}}. \tag{8c}$$

It is remarkable that two sets of equations (7) and (8) are in the same format and convenient for the later inverters' physical dimensions extraction. The negative signs in front of K_{12} in Fig. 7(b) and J_{12} in Fig. 8(b) can be neglected in filter design since they do not influence the filter's magnitude responses.

B. Method for Filter Dimension Derivation

To achieve the coupling degrees determined in Section II-A, geometrical dimensions of the I/O and inter-resonator coupling stages can be routinely extracted by Dishal's method [18], [19]. This extraction approach is constrained by an ideal assumption that electrical property of all the coupling stages does not change the resonator's inherent resonant frequency. In our network, two neighboring $\lambda/4$ resonators are coupled via alternative J/K inverters. The J inverters are implemented by the parallel coupled lines and they seem to change the resonator's inherent frequency very slightly. Meanwhile, the semi-lumped through-via not only provides a short-circuited ground to the $\lambda/4$ resonator, but also functions as a K inverter. As such, variation in the value of K leads to significant shift of the concerned resonant frequency. With this limitation, an alternate filter dimension extraction method is indispensable.

Equations (9a)–(9c) were initially derived in [20] and are used to transform an asymmetrical two-port susceptance network in Fig. 5(a) to its associated J inverter network in Fig. 5(b). Herein, all the susceptance elements can be extracted from the full-wave-simulated two-port S-parameters

$$\frac{J}{\sqrt{Y_1 Y_2}} = \frac{\sin\left(\frac{-\phi_1}{2}\right) + \bar{B}_{11}\cos\left(\frac{-\phi_1}{2}\right)}{\bar{B}_{12}\sin\left(\frac{-\phi_2}{2}\right)} \tag{9a}$$

$$\phi_1 = M_1\pi + \tan^{-1}\{\frac{2(\bar{B}_{11} + \bar{B}_{22}|\bar{B}|)}{1 + \bar{B}_{22}^2 - \bar{B}_{11}^2 - |\bar{B}|^2}\} \tag{9b}$$

$$\phi_2 = M_2\pi + \tan^{-1}\{\frac{2(\bar{B}_{22} + \bar{B}_{11}|\bar{B}|)}{1 + \bar{B}_{11}^2 - \bar{B}_{22}^2 - |\bar{B}|^2}\} \tag{9c}$$

where $\bar{B}_{11} = B_{11}/Y_1$, $\bar{B}_{22} = B_{22}/Y_2$, and $\bar{B}_{12} = B_{12}/\sqrt{Y_1 Y_2}$, and $|\bar{B}| = \bar{B}_{11}\bar{B}_{22} - \bar{B}_{12}^2$, Y_1, and Y_2 are the characteristic admittances of two ports, M_1 and M_2 are the two non-negative integers. Meanwhile [16, eq. (3)] is capable to extract the equivalent asymmetrical network of the K inverter in Fig. 5(c) based on the asymmetrical two-port reactance network. These two sets of equations could certainly be utilized to extract dimensions of J and K inverters with the aid of a commercial full-wave electromagnetic (EM) simulator. With scrutinizing the network in Fig. 5(b), the middle J inverter can be directly changed with the K inverter in Fig. 5(c) based on their relationship as

$$\frac{K}{\sqrt{Z_1 Z_2}} = \frac{\sqrt{Y_1 Y_2}}{J} = \frac{\bar{B}_{12}\sin\left(\frac{-\phi_2}{2}\right)}{\sin\left(\frac{-\phi_1}{2}\right) + \bar{B}_{11}\cos\left(\frac{-\phi_1}{2}\right)} \tag{10}$$

where $Z_1 = 1/Y_1$ and $Z_2 = 1/Y_2$. Both effective lengths $\phi_1/2$ and $\phi_2/2$ are kept unchanged so that dimensions of both J and K inverters can be extracted from the susceptance network, as portrayed in Fig. 5(a) alone.

According to the above discussion, all the dimensions of J and K inverters and their respect effective electrical lengths are determined. The next step is to insert different lengths of transmission-line segments between J and K inverters to form the complete effective quarter-wavelength resonators. Since the aforementioned dimension extraction procedure is executed via the full-wave simulation, extracted parameters have included all the parasitic effects, such as junction effects and end effects, the final layout of the designed filter can be simply determined with a rapid fine-tuning procedure.

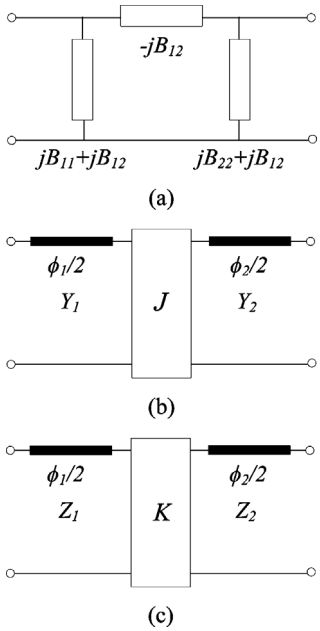

Fig. 5. (a) Two-port π-type susceptance network. (b) Equivalent J inverter network. (c) Equivalent K inverter network with asymmetrical geometry.

III. Synthesis of Fourth-Order Microstrip Bandpass Filter

In this section, detail synthesis for the fourth-order Chebyshev bandpass filter in Fig. 4(a), implemented on microstrip-line structure, will be demonstrated. The used substrate is a Roger's RT/Duriod 6010 with $\epsilon_r = 10.8, \tan\delta = 0.002$, and thickness $=$ 1.27 mm. The prescribed filter is centered at frequency $f_0 =$ 2.4 Ghz with a fractional bandwidth of 10% and return loss of 20 dB in the passband. Due to the symmetrical geometry of the constituted even-order Chebyshev bandpass filters, both the I/O port impedances are set as $Z_0 = 50\ \Omega$ and they are used for the J/k inverters' dimension extraction in (9a) and (10). On the contrary, characteristic impedance of all the $\lambda/4$ resonators can be any value. Based on (7a)–(7c),

$$\frac{J_{01}}{Y_0} = \sqrt{\frac{\mathrm{FBW}\pi}{4g_0g_1}} = 0.2904 \tag{11a}$$

$$-\frac{K_{12}}{Z_0} = \frac{J_{12}}{Y_0} = \frac{\mathrm{FBW}\pi}{4}\sqrt{\frac{1}{g_1g_2}} = 0.07160 \tag{11b}$$

$$\frac{J_{23}}{Y_0} = \frac{\mathrm{FBW}\pi}{4}\sqrt{\frac{1}{g_2g_3}} = 0.05501 \tag{11c}$$

where g_n are the first four elements of fourth-order Chebysehv low-pass, $g_0 = 1, g_1 = 0.9314, g_2 = 1.2920$, and $g_3 = 1.5775$.

The width of the $\lambda/4$ microstrip line is chosen as 0.6 mm with the characteristic impedance of $Z_r = 64.21\ \Omega$. The inset figure in Fig. 6(a) shows the layout of the K_{12} inverter in the form of the through-via, the diameter of the through-via and the width of the shunt stub are set as 0.7 and 1.0 mm, respectively. The stub length, D, is defined as the distance between the microstrip edge and the center of

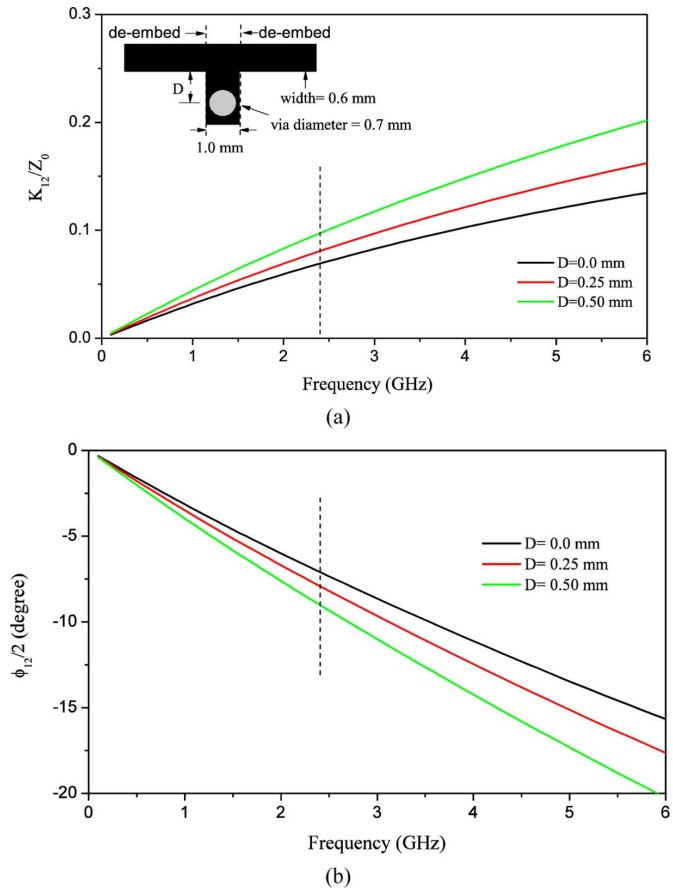

Fig. 6. Dimension derivation of K_{12} inverter. (a) Normalized K_{12} with Z_0. (b) Effective length $\phi_{12}/2$ as a function of frequency with stub length D.

via. Fig. 6(a) portrays the extracted normalized K_{12} with $Z_0 = 50\ \Omega$ using (10) as D increases from 0 to 0.25 and 0.50 mm. Of them, $D = 0.25$ mm is chosen based on the absolute value indicated in (11b) at 2.4 GHz, and its associated effective electrical length is found as $\phi_{12}/2 = -7.9°$.

To construct the other coupling stages with J_{01} and J_{23}, their effective electrical lengths must be less than 82.1° (90°–7.9°). Therefore, the coupling lengths of J_{01} and J_{23} are both chosen as 10.5 mm, which matches the uncoupled electrical length of 79.1° as calculated by the LineCalc in the Agilent Advanced Design System (ADS). Coupling spaces extraction of J_{01} and J_{23} are performed based on (9) and (11a)–(11c) with the fixed coupling length of 10.5 mm. According to the results shown in Fig. 7 for J_{01} and Fig. 8 for J_{23}, the coupling spaces for these two stages are chosen as 0.7 and 2.75 mm, respectively. Their extracted effective electrical lengths are $\phi_{01}/2 = -80.2°$ and $\phi_{23}/2 = -79.25°$, and their absolute values are slightly longer than uncoupled electrical length of 79.1°. The effective length of the J_{01} stage is longer than the one of the J_{23} stage due to its stronger coupling strength.

With the determination of physical dimensions and their associated effective lengths of both J and K inverters, different microstrip line segments are inserted between the alternative J/K inverter to form an effective $\lambda/4$ resonator. To avoid the discontinuity, the microstrip line with a width of 0.6 mm is chosen.

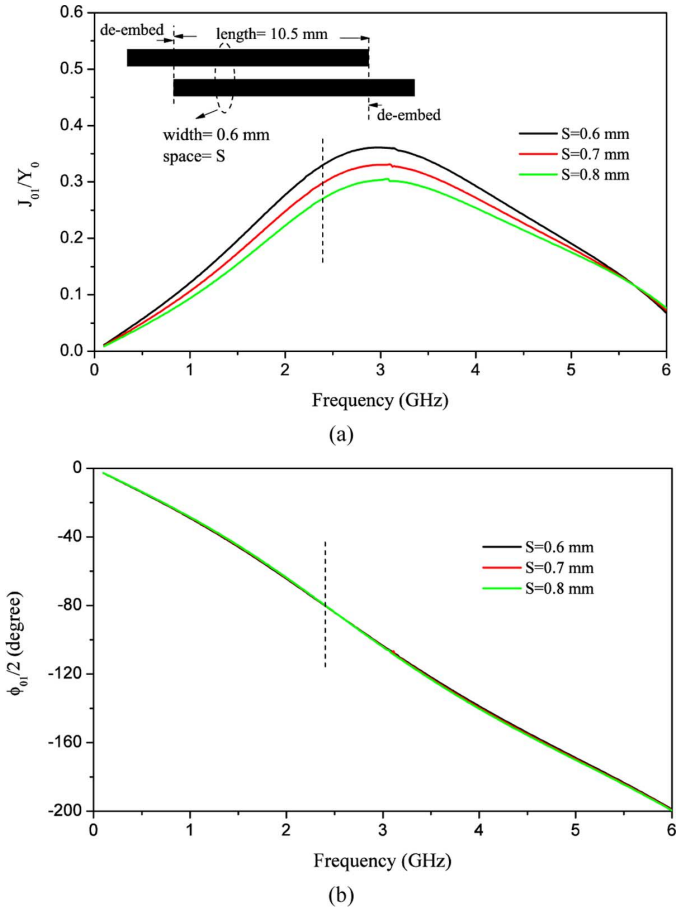

Fig. 7. (a) Extracted normalized values and (b) effective electrical lengths of J_{01} as a function of frequency with different coupling gap S.

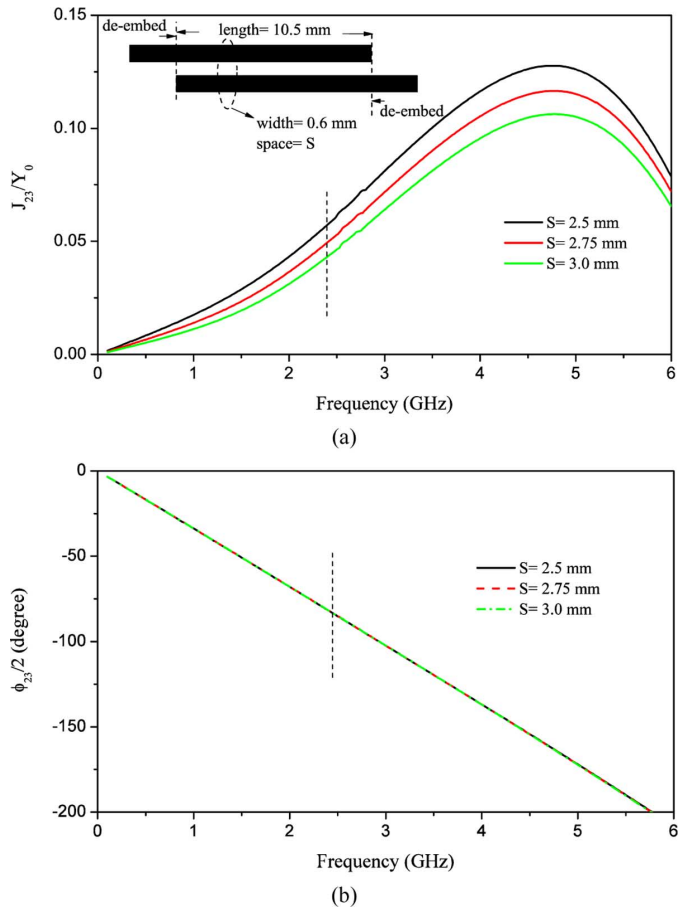

Fig. 8. (a) Extracted normalized values and (b) effective electrical lengths of J_{12} as a function of frequency with different coupling gap S.

Fig. 9 shows the schematic of a resultant first-stage effective $\lambda/4$ resonator that is composed of three distinct segments with

$$Z_L = \frac{Z_0}{j\tan\left(\frac{|\phi_{01}|}{2}\right)} \tag{12a}$$

$$Z_R = jZ_0\tan\left(\frac{|\phi_{12}|}{2}\right) \tag{12b}$$

$$Z_R^s = Z_r\frac{Z_R + jZ_{r\tan(|\phi_1^s|)}}{Z_r + jZ_{R\tan(|\phi_1^s|)}}. \tag{12c}$$

Applying the resonant condition,

$$Z_L + Z_R^s = 0. \tag{13}$$

The electrical compensated lengths of the first and second $\lambda/4$ resonators can be calculated as $\phi_1^s = 1.5°$ and $\phi_2^s = 2.24°$, and their physical lengths are found as 0.20 and 0.30 mm using the LineCalc in ADS. Since the filter is symmetrical with the central J_{23} inverter, the filter layout can be preliminarily determined.

Based on the above-described procedure, an initial fourth-order Chebyshev bandpass filter on $\lambda/4$ resonators is designed and the photograph of the first fabricated filter with the detailed dimensions after minor fine tuning is illustrated in Fig. 10(a).The inset figure in Fig. 10(b) plots the three sets of

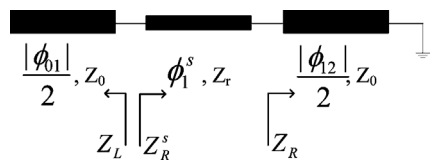

Fig. 9. Electrical compensated length extraction for the first $\lambda/4$ resonator.

frequency responses, which are derived from the synthesis-oriented network, full-wave simulated results of the filter layout and measurement of the fabricated filter circuit, respectively. In the core passband, the theoretical and full-wave simulated responses match well with each other due to the presented filter dimension extraction method. The measured in-band insertion and return losses are found to be 2.78 and 11.1 dB, respectively. Visible discrepancy between the simulated and measured results may be caused by the inaccurate permittivity of the dielectric substrate, the unexpected fabrication tolerance and the transition losses in measurement.

Since the filter is designed based on $\lambda/4$ resonators, the first spurious response happens at 7.2 GHz, i.e., $3f_0$. Outside the core passband, there are two transmission zeros located at the both sides of the core passband although the right transmission zero is not clearly observable in the simulated results. Coupling route with parasitic weak cross couplings of the bandpass filter in Fig. 10(a) needs to be investigated using the diagram in Fig. 11(b). The mainline coupling $(J_{s1} - K_{12} - J_{23})$ is in

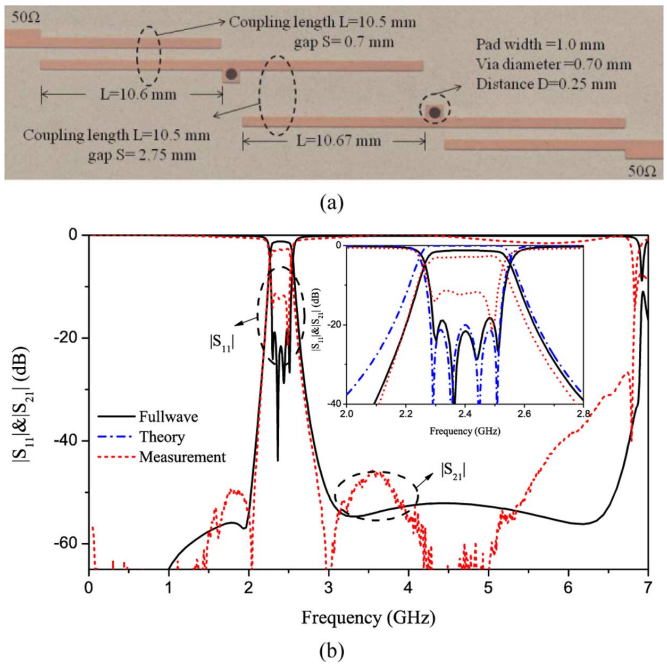

Fig. 10. (a) Photograph of fabricated fourth-order Chebyshev bandpass filter. (b) Comparison among the simulated, theoretical and measured S-parameters.

the form of alternative J/K inverters, whereas the weak cross coupling J_{s3} between source (S) and resonant node 3 is out-of-phase with the mainline coupling route at certain frequencies, which can be considered as a quadruplet section. Meanwhile, there is another quadruplet section among the resonant nodes 2–4 and the load (L). Thus, locations of such transmission zeros could be adjusted and controlled by varying the cross-coupling strengths J_{s3} and J_{2L}. Fig. 11(a) shows a photograph of a modified Chebyshev bandpass filter. As compared to the initial filter in Fig. 10(a), the second and fourth $\lambda/4$ resonators are bent downwards and upwards by 30° in order to get the improved filtering performance. As shown in Fig. 11(c), two transmission zeros are located at 2.15 and 2.78 GHz, as can be clearly seen in Fig. 11(c) for both full-wave simulated and measured results. If these two transmission zeros are put much closer to the core passband, the resultant passband does not strictly function as a Chebyshev frequency response. The respective J and K inverters need to be determined from the coupling matrix $\boldsymbol{m}$ with the prescribed generalized-Chebyshev in-band frequency response [21]. Transmission zeros at 4.5 GHz in Fig. 10(b) and 4.9 GHz in Fig. 11(c) are mainly attributed by capacitive S/L cross couplings.

By applying the same extraction procedure, the dual fourth-order Chebyshev bandpass filter, as portrayed in Fig. 4(b), is designed at 2.4 GHz with a fractional bandwidth of 10% and return loss of 20 dB in the passband. All the microstrip-line resonators are chosen as 1.1 mm in their strip width, which results in the characteristic impedance equal to the source/load impedance of 50 Ω. The transformed normalized values of J/K inverters can be calculated according to (8), and their values are given in (14a)–(14c) as follows:

$$\frac{K_{01}}{Z_0} = \sqrt{\frac{\mathrm{FBW}\pi}{4g_0g_1}} = 0.2904 \tag{14a}$$

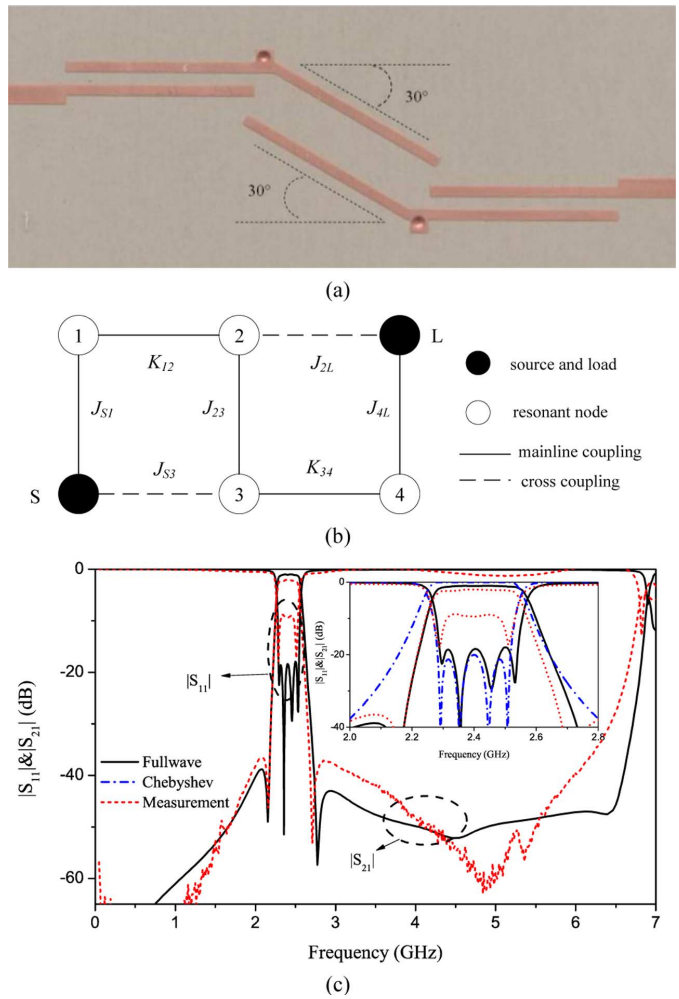

Fig. 11. (a) Photograph of fabricated fourth-order filter with modified configuration. (b) Coupling and routing diagram. (c) Comparison among the simulated, theoretical, and measured S-parameters.

$$-\frac{J_{12}}{Y_0} = \frac{Z_{12}}{Z_0} = \frac{\mathrm{FBW}\pi}{4}\sqrt{\frac{1}{g_1g_2}} = 0.07160 \tag{14b}$$

$$\frac{K_{23}}{Z_0} = \frac{\mathrm{FBW}\pi}{4}\sqrt{\frac{1}{g_2g_3}} = 0.05501. \tag{14c}$$

The resultant filter layout with denoted dimensions is shown in Fig. 12(a). The required coupling parameter, K_{23}/Z_0, is as weak as 0.05501, which results in the via diameter as large as 0.83 mm. Instead of a single via, in practical implementation, multiple vias connected in parallel or two closely spaced vias can be deployed to realize the weaker K values as specified. As can be seen in Fig. 12(b), a simulated in-band frequency response is almost the same as the theoretical Chebyshev frequency response. Measured in-band insertion and return losses are 2.98 and 9.87 dB, which are mainly due to the inaccurate substrate permittivity, the unexpected fabrication tolerance and transition losses in the measurement. The measured transmission zeros at 1.75 and 4.5 GHz are primarily attributed by the weak out-of-phase cross coupling among the first and fourth $\lambda/4$ resonators with the mainline counterpart. The first spurious response is noticed around 7.2 GHz. The measured and simulated wideband frequency responses also match well, as plotted in Fig. 12(b).

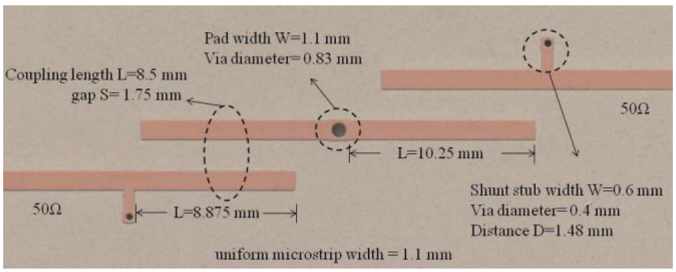

(a)

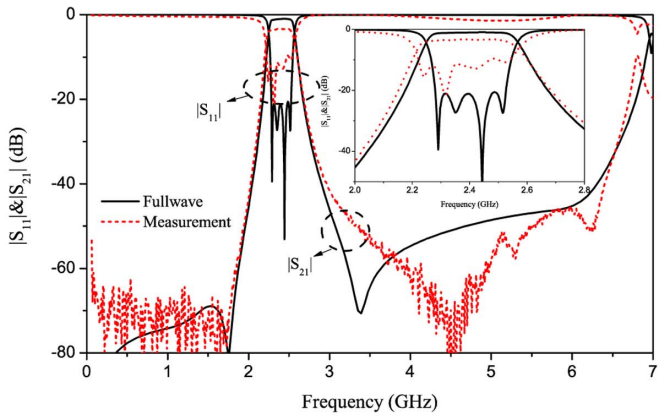

(b)

Fig. 12. (a) Photograph of second fourth-order Chebyshev bandpass filter based on $\lambda/4$ resonators. (b) Comparison between simulated and measured results.

IV. Synthesis of Sixth-Order Microstrip Bandpass Filter

In this section, a sixth-order Chebyshev bandpass filter is designed at 2.4 GHz with the fractional bandwidth 15%. According to [1], the first five elements of sixth-order Chebyshev low-pass, $g_0 = 1$, $g_1 = 0.9940$, $g_2 = 1.4131$, $g_3 = 1.8933$, $g_4 = 1.5506$ for the 20-dB in-band return loss. For the same substrate used above, the strip width of microstrip resonators is kept as 0.6 mm, which results in the characteristic impedance $Z_r = 64.21\ \Omega$. Hence, the values of normalized J/K inverters with respect to the port impedance Z_0 can be calculated as follows based on (7):

$$\frac{J_{01}}{Y_0} = \sqrt{\frac{\mathrm{FBW}\pi}{4g_0g_1}} = 0.3443 \tag{15a}$$

$$-\frac{K_{12}}{Z_0} = \frac{J_{12}}{Y_0} = \frac{\mathrm{FBW}\pi}{4}\sqrt{\frac{1}{g_1g_2}} = 0.09940 \tag{15b}$$

$$\frac{J_{23}}{Y_0} = \frac{\mathrm{FBW}\pi}{4}\sqrt{\frac{1}{g_2g_3}} = 0.07203 \tag{15c}$$

$$-\frac{K_{34}}{Z_0} = \frac{J_{34}}{Y_0} = \frac{\mathrm{FBW}\pi}{4}\sqrt{\frac{1}{g_3g_4}} = 0.06876. \tag{15d}$$

As the physical dimensions of K_{12} and K_{34} are extracted based on (10), (15b), and (15d), their preliminary physical dimensions can be derived, as indicated in Fig. 13(a), over which their associated effective lengths are $-8.90°$ and $-6.57°$, respectively. The coupling length for J_{01} and J_{23} is then fixed as 9.0 mm so that the coupling zero of this coupled line section can be employed to suppress the spurious at $3f_0$ [12]. Each coupling space

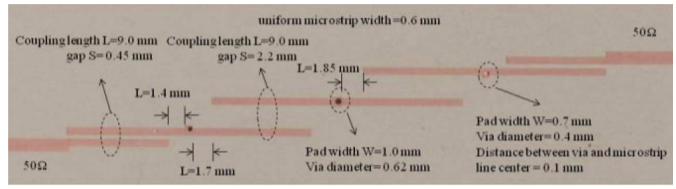

(a)

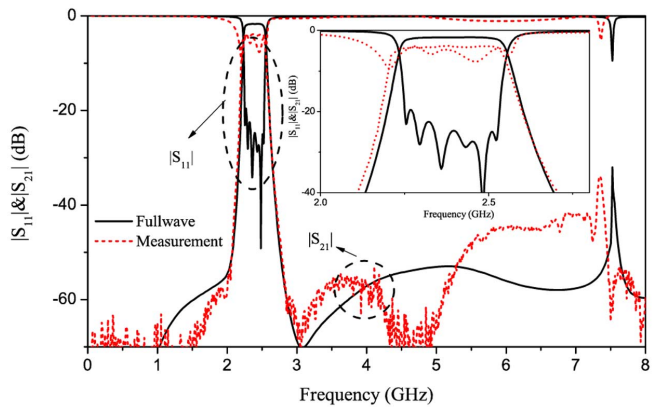

(b)

Fig. 13. (a) Photograph fabricated sixth-order Chebyshev bandpass filter with detail dimensions. (b) Comparison between simulated and measured results.

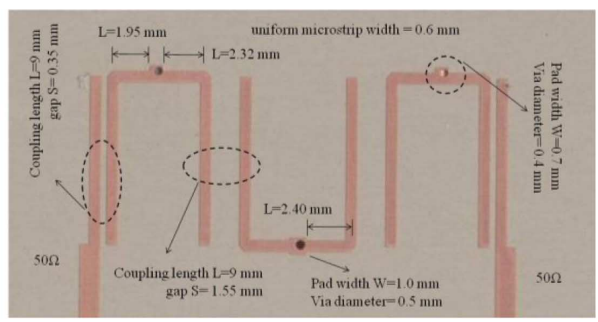

(a)

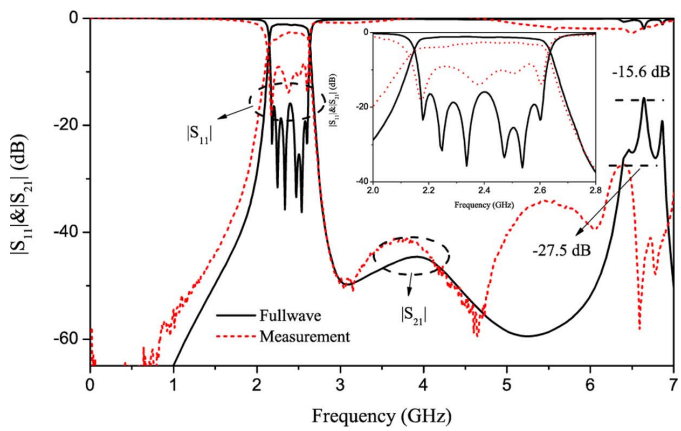

(b)

Fig. 14. (a) Photograph of the fabricated sixth-order hairpin Chebyshev bandpass filter. (b) Comparison between simulated and measured results.

is tuned to achieve the coupling strength as specified in (15a) and (15c), and the coupling gaps of J_{01} and J_{23} are determined as 0.45 and 2.2 mm, their extracted effective lengths are 68.0° and 65.7°. Next, the compensated electrical or physical lengths

for the first, second, and third resonators are calculated based on (13) as $\phi_1^s = 10.51^\circ$ or 1.41 mm, $\phi_2^s = 12.42^\circ$ or 1.65 mm, and $\phi_3^s = 14.25^\circ$ or 1.90 mm. Hence, the overall filter layout can be determined, and the final layout is displayed in Fig. 13(a) after minor fine tuning.

The full-wave simulated and measured frequency responses are portrayed in Fig. 13(b). The simulated return loss is higher than 20 dB within the 15% passband, and the six transmission poles are clearly demonstrated. However, due to the inaccurate substrate permittivity, the unexpected fabrication tolerance and transition losses in the measurement, the measured in-band return and insertion losses are 3.77 and 4.15 dB, respectively. The measured results still show a relatively flat passband. The spurious response at 7.2 GHz is below -30 dB due to emergence of coupling zeros caused by the three J inverters around 7.2 GHz [12]. Since the sixth-order bandpass filter possesses relatively sharp rejection ratios and out-of-band suppression, the plural transmission zeros are not sharply obvious. As in the fourth-order bandpass filters, these finite transmission zeros are also attributed to the out-of-phase cross couplings, such as the capacitive cross coupling between second and fifth resonators. Nevertheless, the measured results reasonably match with the theoretical ones.

To save the circuit area, the conventional straight $\lambda/2$ microstrip line resonators are then reshaped as the compact hairpin units. Similarly, the filter structure with the area of $(48.2\ \text{mm}^*8.3\ \text{mm})$ in Fig. 13(a) is modified to create a resultant bandpass filter based on the $\lambda/4$ hairpin units with the circuit area of $(22.44\ \text{mm}^*9.6\ \text{mm})$, as displayed in Fig. 14(a). By comparing them, the overall area of the filter is reduced by 46%. A previous filter dimension derivation method does not take into account of the complicated parasitic couplings existing in the hairpin bandpass filter, but it still provides a close preliminary filter layout dimensions. With the aim of the flat passband, simulated in-band insertion loss is as good as 20 dB, and fractional bandwidth is around 18.5% after performing fine tuning, which is wider than the prescribed 15.0%. The measure in-band return and insertion losses are 9.13 and 2.74 dB. The measured results match reasonably well with its theoretical ones.

V. Conclusion

In this paper, we propose a detail synthesis method for the even-order Chebyshev bandpass filter based on the $\lambda/4$ microstrip line resonators and alternative J/K inverters. The values of alternative J and K are transformed from the conventional all J or all K filter prototypes. The overall filter dimension extraction method is explicitly and effectively demonstrated to facilitate the synthesis design of the fourth- and sixth-order Chebyshev bandpass filters. Two groups of Chebyshev bandpasss filters with the fourth- and sixth-order number are designed and fabricated. The measured frequency responses for the fabricated filters have well justified the synthesis design method for the even-order symmetrical bandpass filters with a Chebyshev frequency response.

References

[1] G. Matthaei, L. Young, and E. Jones, *Microwave Filters, Impedance-Matching Networks, and Coupling Structures*. Norwood, NA: Artech House, 1980.

[2] G. Matthaei, "Direct-coupled, bandpass filters with $\lambda/4$ resonators," in *Int. IRE Conf. Rec.*, Mar. 1958, vol. 6, pp. 98–111.

[3] T. Tsujiguchi, H. Matsumoto, and T. Nishikawa, "A miniaturized end-coupled bandpass filter using $\lambda/4$ hair-pin coplanar resonators," in *IEEE MTT-S Int. Microw. Symp. Dig.*, 1998, vol. 2, pp. 829–832.

[4] J. Gao and L. Zhu, "Asymmetric parallel-coupled CPW stages for harmonic suppressed $\lambda/4$ bandpass filters," *Electron. Lett.*, vol. 40, no. 18, pp. 1122–1123, Sep. 2004.

[5] F. Aryanfar and K. Sarabandi, "Characterization of semilumped CPW elements for millimeter-wave filter design," *IEEE Trans. Microw. Theory Techn.*, vol. 53, no. 4, pp. 1288–1293, Apr. 2005.

[6] J. Zhou, M. Lancaster, and F. Huang, "Coplanar quarter-wavelength quasi-elliptic filters without bond-wire bridges," *IEEE Trans. Microw. Theory Techn.*, vol. 52, no. 4, pp. 1150–1156, Apr. 2004.

[7] Z. Ma, H. Suzuki, Y. Kobayashi, K. Satoh, S. Narahashi, and T. Nojima, "A low-loss 5 GHz bandpass filter using HTS coplanar waveguide quarter-wavelength resonators," in *IEEE MTT-S Int. Microw. Symp. Dig.*, 2002, vol. 3, pp. 1967–1970.

[8] H. Kanaya, K. Kawakami, F. Koga, Y. Kanda, and K. Yoshida, "Design and performance of miniaturized quarter-wavelength resonator bandpass filters with attenuation poles," *IEEE Trans. Appl. Supercond.*, vol. 15, no. 2, pp. 1016–1019, Jun. 2005.

[9] J. R. Lee, J. H. Cho, and S. W. Yun, "New compact bandpass filter using microstrip $\lambda/4$ resonators with open stub inverter," *IEEE Microw. Guided Wave Lett.*, vol. 10, no. 12, pp. 526–527, Dec. 2000.

[10] C. H. Wang, Y. S. Lin, and C. Hsiung, "Novel inductance-incorporated microstrip coupled-line bandpass filters with two attenuation poles," in *IEEE MTT-S Int. Microw. Symp. Dig.*, 2004, vol. 3, pp. 1979–1979.

[11] Y. S. Lin, C. H. Wang, C. H. Wu, and C. Hsiung, "Novel compact parallel-coupled microstrip bandpass filters with lumped-element K-inverters," *IEEE Trans. Microw. Theory Techn.*, vol. 53, no. 7, pp. 2324–2328, Jul. 2005.

[12] C. H. Wu, Y. S. Lin, C. H. Wang, and C. Hsiung, "Novel microstrip coupled-line bandpass filters with shortened coupled sections for stopband extension," *IEEE Trans. Microw. Theory Techn.*, vol. 54, no. 2, pp. 540–546, Feb. 2006.

[13] A. Sanada, H. Takehara, and I. Awai, "Design of the CPW in-line $\lambda/4$ stepped-impedance resonator bandpass filter," in *Asia–Pacific Microw. Conf.*, 2001, vol. 2, pp. 633–636.

[14] S. C. Lin, T. N. Kuo, Y. S. Lin, and C. Hsiung, "Novel coplanar-waveguide bandpass filters using loaded air-bridge enhanced capacitors and broadside-coupled transition structures for wideband spurious suppression," *IEEE Trans. Microw. Theory Techn.*, vol. 54, no. 8, pp. 3359–3369, Aug. 2006.

[15] S. C. Lin, "Microstrip dual/quad-band filters with coupled lines and quasi-lumped impedance inverters based on parallel-path transmission," *IEEE Trans. Microw. Theory Techn.*, vol. 59, no. 8, pp. 1937–1946, Aug. 2011.

[16] S. Zhang, L. Zhu, and R. Li, "Compact quadruplet bandpass filter based on alternative J/K inverters and $\lambda/4$ resonators," *IEEE Microw. Wireess Compon. Lett.*, vol. 22, no. 5, pp. 224–226, May 2012.

[17] I. C. Hunter, *Theory and Design of Microwave Filters*. London, U.K.: Inst. Eng. Technol., 2006.

[18] M. Dishal, "Alignment and adjustment of synchronously tuned multiple-resonant-circuit filters," *Proc. IRE*, vol. 39, no. 11, pp. 1448–1455, Nov. 1951.

[19] J. Hong and M. Lancaster, *Microstrip Filters for RF/Microwave Applications*. New York: Wiley, 2001.

[20] L. Zhu and K. Wu, "Accurate circuit model of interdigital capacitor and its application to design of new quasi-lumped miniaturized filters with suppression of harmonic resonance," *IEEE Trans. Microw. Theory Techn.*, vol. 48, no. 3, pp. 347–356, Mar. 2000.

[21] R. J. Cameron, "General coupling matrix synthesis methods for Chebyshev filtering functions," *IEEE Trans. Microw. Theory Techn.*, vol. 47, no. 4, pp. 433–442, Apr. 1999.

Songbai Zhang (S'11) was born in Jiangsu Province, China. He received the B.Eng. degree from Nanyang Technological University (NTU), Singapore, in 2010, and is currently working toward the Ph.D. degree in electrical and electronic engineering at NTU.

His research interests include microwave passive filter design.

Mr. Zhang was the recipient of Ministry of Education Scholarship (2006–2010), Singapore, and an NTU Research Scholarship (2010–2014).

Lei Zhu (S'91–M'93–SM'00-F'12) received the B.Eng. and M.Eng. degrees in radio engineering from the Nanjing Institute of Technology (now Southeast University), Nanjing, China, in 1985 and 1988, respectively, and the Ph.D. Eng. degree in electronic engineering from the University of Electro-Communications, Tokyo, Japan, in 1993.

From 1993 to 1996, he was a Research Engineer with Matsushita-Kotobuki Electronics Industries Ltd., Tokyo, Japan. From 1996 to 2000, he was a Research Fellow with the École Polytechnique de Montréal, University de Montréal, Montréal, QC, Canada. Since July 2000, he has been an Associate Professor with the School of Electrical and Electronic Engineering, Nanyang Technological University, Singapore. He has authored or coauthored over 215 papers in peer-reviewed journals and conference proceedings. His papers have been cited more than 2300 times with an H-index of 25 (source: ISI Web of Science). He was an Associate Editor for the *IEICE Transactions on Electronics* (2003–2005). His research interests include planar filters, planar periodic structures, planar antennas, numerical EM modeling, and deembedding techniques.

Dr. Zhu has been an associate editor for the IEEE MICROWAVE AND WIRELESS COMPONENTS LETTERS (MWCL) since October 2006 and an associate editor for the IEEE TRANSACTIONS ON MICROWAVE THEORY AND TECHNIQUES (TMTT) since June 2010. He has been a member of the IEEE Microwave Theory and Techniques Society (IEEE MTT-S) Technical Committee 1 on Computer-Aided Design since June 2006. He was a general chair of the 2008 IEEE MTT-S International Microwave Workshop Series (IMWS'08) on the Art of Miniaturizing RF and Microwave Passive Components, Chengdu, China, and a Technical Program Committee (TPC) chair of the 2009 Asia–Pacific Microwave Conference (APMC'09), Singapore. He was the recipient of the 1997 Asia–Pacific Microwave Prize Award, the 1996 Silver Award of Excellent Invention from Matsushita–Kotobuki Electronics Industries Ltd., and the 1993 First-Order Achievement Award in Science and Technology from the National Education Committee, China.